Validation of an engineering model for vortex generators in a viscous-inviscid interaction method for airfoil analysis

Sahoo, Abhratej; Ferreira, Carlos Simao; Ravishankara, Akshay Koodly; Schepers, Gerard; Yu, Wei

DOI
10.1088/1742-6596/2647/11/112012

Publication date
2024

Document Version
Final published version

Published in
Journal of Physics: Conference Series

Citation (APA)
Sahoo, A., Ferreira, C. S., Ravishankara, A. K., Schepers, G., & Yu, W. (2024). Validation of an engineering model for vortex generators in a viscous-inviscid interaction method for airfoil analysis. *Journal of Physics: Conference Series*, *2647*(11), Article 112012. https://doi.org/10.1088/1742-6596/2647/11/112012

Validation of an engineering model for vortex generators in a viscous-inviscid interaction method for airfoil analysis

Journal of Physics: Conference Series **2647** (2024) 112012 doi:10.1088/1742-6596/2647/11/112012

Validation of an engineering model for vortex generators in a viscous-inviscid interaction method for airfoil analysis

Abhratej Sahoo[1,2], Carlos Simao Ferreira [2], Akshay Koodly Ravishankara [1], Gerard Schepers[1], Wei Yu[2]

[1]Wind Energy, TNO Energy and Materials Transition; [2]Wind Energy, TU Delft Aerospace Engineering

E-mail: Abhratej Sahoo (abhratej.sahoo@tno.nl)

Abstract. As the demand for renewable energy increases, wind turbine rotors will become larger with slender blades. Vortex Generators (VGs) are used for passive flow control to avoid flow separation and reduce unsteady loading on the thick root section of slender blades due to their simplicity, inexpensiveness, and the ability to retrofit them to blades. Aerodynamic load calculations for VGs involve long experimental campaigns or resource intensive CFD calculations. Due to their inherent time-intensive nature aeroelastic optimisation and design tools prefer to use simplified but accurate analysis tools for aerodynamic load calculations of clean airfoils. One such class of tools are viscous-inviscid interaction solvers that use Integral Boundary Layer (IBL) methods for viscous calculations in the boundary layer coupled with an inviscid solver for the rest of the domain. The most popular example of this tool is XFOIL. An engineering model for VGs in IBL methods has previously been developed and implemented in XFOIL. In this research, the model parameters are tuned for implementation in another tool RFOIL based on XFOIL. RFOIL has been developed for accurate and robust analysis of wind turbine airfoils with improvements for thick airfoils and rotational corrections. The aerodynamic performance predicted the VG model in both XFOIL and RFOIL is then validated with an extensive database of airfoil data consisting of airfoils between 21% to 60% thickness, as well as Reynolds numbers between 1 million to 14 million, equipped with and without VGs. Finally, the computation time for the VG model is compared with that for a clean airfoil analysis in the same viscous-inviscid interaction solvers RFOIL and XFOIL. The investigation provides an overview of the usability of the engineering model in airfoil design methodologies in the wind turbine industry.

1. Introduction

Studies on the projected capacity of future wind turbine rotors indicate an increasing trend for bigger rotors with smaller induction and slender blades [1; 2]. Thick airfoils [2] and thick trailing edges [3] balance the structural loads on inboard sections. However, these sections have a higher sensitivity to flow separation and leading edge roughness. This directly affects the turbine's annual energy production, increasing the levelised cost of energy [4]. Moreover, fluctuations from separated flow around these sections lead to higher fatigue loads. Passive technologies to delay flow separation are still preferred over active control and redesign due to their simplicity and ability to retrofit standard blades with static add-ons. Vortex Generators (VGs) are one

of the oldest and most studied ways to delay flow separation [5; 6]. Optimising passive VG arrays involves extensive parametric studies through experiments or computations. Typically, flow around VGs is computed using CFD analyses of complexity varying from fully resolved approaches with body-fitted domains, to partly modelled and partly resolved approaches like the BAY model [7; 8]. These methods still require a large computation time, despite recent advances in computational capacity. In contrast, when dealing with airfoils without VGs, most airfoil and blade design routines employ lower fidelity airfoil analysis tools like XFOIL [9], or its variations like RFOIL [10] for fast and reliable estimation of lift, drag, and moments. RFOIL is specifically tuned for thicker airfoil sections with improved lift and drag prediction and rotational corrections [11–13], making it a more accurate tool for airfoil design for wind turbines.

Both RFOIL and XFOIL couple an inviscid panel method and a viscous solver based on Integral Boundary Layer (IBL) methods [14] with appropriate viscous-inviscid interaction schemes. In the past, VGs have been modelled in these IBL methods as an additional source of turbulence in the boundary layer [15]. An implementation of this idea in XFOIL resulted in XFOILVG [16], where the added turbulence was expressed in the transport equation for turbulent shear stress as a source term calculated via multivariate regression using lift polars of several airfoil sections. The present work has implemented the VG model in the improved tool RFOIL. Following this, the present work examines the validity of modelling VGs as an added source of turbulence in boundary layers by bench-marking the VG model in both RFOIL and XFOIL against lift polars of an extensive database of airfoil sections with different VG arrays.

2. Description of the engineering model

For an incompressible turbulent boundary layer, integral boundary layer codes solve three governing equations (Equations (1) to (3)) — the first describing the transport of momentum in the boundary layer, the second describing the transport of kinetic energy in the boundary layer, and the third describing the evolution of turbulent shear stress in the boundary layer. The last equation is also called the shear lag equation because it quantifies the lag in shear stress between the turbulent boundary layer and an equilibrium state. Equilibrium flows are defined as flows in which the shape of the velocity and shear-stress profiles in the boundary layer do not vary with the streamwise location [17].

$$\frac{\mathrm{d}\theta}{\mathrm{d}x} = \frac{\mathrm{C_f}}{2} - (\mathrm{H}+2)\,\frac{\theta}{\mathrm{u_e}}\frac{\mathrm{du_e}}{\mathrm{d}x} \tag{1}$$

$$\frac{\mathrm{d}H_k}{\mathrm{d}x} = \frac{2\mathrm{C_{\mathcal{D}}}}{\theta} - \frac{H_k}{\theta}\frac{\mathrm{C_f}}{2} - (1-H)\,\frac{H_k}{\mathrm{u_e}}\frac{\mathrm{du_e}}{\mathrm{d}\xi} \tag{2}$$

$$\frac{\delta}{C_\tau}\frac{dC_\tau}{d\xi} = K_c\left(C_{\tau_{EQ}}^{1/2} - C_\tau^{1/2}\right) \tag{3}$$

To model the added turbulence due to VGs in the boundary layer, de Tavernier et al. included a source term to the equilibrium shear stress coefficient $C_{\tau_{EQ}}$ in the shear lag equation, modelling the tendency of the VG-influenced boundary layer to deviate from an equilibrium state. Thus,

$$\frac{\delta}{C_\tau}\frac{dC_\tau}{d\xi} = K_c\left(\left(C_{\tau_{EQ}}^{1/2} + S_{VG}\right) - C_\tau^{1/2}\right), \quad \text{where:} \quad S_{VG} = \begin{cases} 0, & x < x_{VG} \\ \sigma_0 e^{-\lambda(x-x_{VG})}, & x \geq x_{VG} \end{cases} \tag{4}$$

The source term was evaluated through a multivariate regression scheme for geometric parameters of VG arrays using lift polars of several airfoil sections. The parametric dependence of the source term on VG geometry and the incoming flow is given by Equation (5), where $C_0 \ldots C_3$ are constants from the multivariate regression. The source term depends on VG geometric parameters like height h, length l, inclination angle β (shown in Figure 1), as well the

velocity at the tip of the VG vane U_{VG}. U_{VG} is characteristic of the incoming boundary layer flow and is reconstructed from the Reynolds number Re_θ using the Swafford velocity profile [18].

$$I_{ST} = \int_0^1 S_{VG} \mathrm{d}(x/c) = C_0 \cdot \left(\frac{h}{c}\right)^{C_1} \cdot \left(\frac{l}{c} \cdot \sin\beta\right)^{C_2} \cdot (U_{VG})^{C_3} \tag{5}$$

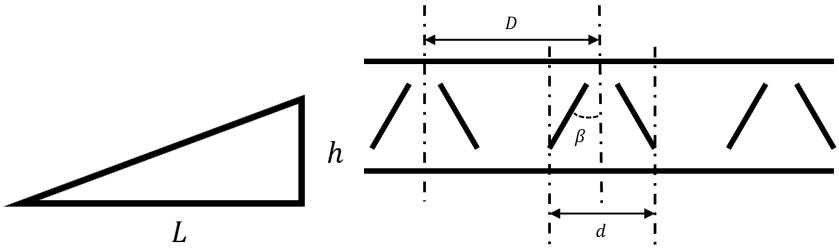

(a) Vane geometry (b) Array geometry

Figure 1: VG geometry parameters

In addition, the model assumes that a laminar boundary layer transitions to a turbulent boundary layer at the VG location. In IBL solvers, this usually means switching from laminar closures to turbulent closures for the governing equations.

Since the IBL solver implemented in RFOIL differs slightly from XFOIL because of its improvements for wind energy applications, the model constants of the VG model $C_0 \dots C_3$ are also different in RFOILVG compared to XFOILVG.

3. Approach and description of reference data sets

The validation of the VG model was performed in three stages. First, since the model constants had to be recalibrated for implementation in RFOIL compared to XFOIL, the expected effects of equipping airfoils with VGs were verified against clean airfoils without VGs. As expected, stall is delayed and maximum lift is higher for an airfoil with VGs than without, as seen in Figure 2. Following this, some baseline statistics were established for appropriate comparison. Since baseline RFOIL is still better than baseline XFOIL without the VG model, a large database of airfoil polars without VGs was generated. This serves as the baseline to compare whether the VG model performs better or worse for calculating airfoil polars. Finally, the VG model was benchmarked against experimental and CFD data sets of airfoils equipped with VGs. The details of some selected data sets are provided below to demonstrate the extensive range of airfoil thicknesses, Reynolds numbers, and VG configurations for which the VG model is benchmarked.

3.1. TU Delft data set [19; 20]

The TU Delft data set consists of polars of the DU-93-W-210, DU-91-W2-250, and DU-97-W-300 airfoils acquired in the low-turbulence tunnel at TU Delft. The flow Reynolds number was between 1 million to 3 million with an inflow turbulence intensity between 0.02% at $Re = 1 \times 10^6$ to 0.07% at $Re = 3 \times 10^6$. These values were used to calculate the critical amplification factor for the e^N transition method [21] for cases of free transition. Fixed transition was also provided using zigzag tapes. An extensive variation of VG arrays varying the chord-wise location, spacings between the vanes and inclination angles has been tested. The wind tunnel data was corrected for solid and wake blockage due to the wind tunnel walls, as well as streamline curvature effects.

This data set was used to calibrate the VG model and as such is not included in the benchmark process. Since the model is calibrated using a multivariate regression scheme based on a least

squares approach, variance in lift predictions still exists when bench-marking the model with this data set. This variance is used as the baseline variance for the VG model in XFOIL and RFOIL.

3.2. RISO Wind Tunnel data set [22]

The RISO data set was obtained in a series of experiments performed on the FFAW3241 and the FFAW3301 airfoils in the VELUX wind tunnel in Denmark. The tests were carried out at a Reynolds number of 1.6 million. VGs of heights 0.6% of chord and 1% of chord were mounted on the suction side between 10% to 30% chordwise position for airfoils with and without a zigzag trip tape simulating leading edge roughness. The turbulence intensity at the test section inflow was recorded at 1%. Since the turbulence intensity of the measurements is relatively high, the wind tunnel data could have some uncertainty. The original data is corrected for blockage but not for streamline curvature, citing the use of end plates.

3.3. Stuttgart LWT data set [23]

This data set consists of wind tunnel data from the Stuttgart University Laminar Wind Tunnel. Two airfoil sections FFA-W3-301 and FFA-W3-360 were tested with and without VGs. The flow Reynolds number is 3 million. The VGs consist of a strip of counter-rotating pairs of triangular vanes placed at different locations along the chord. The VGs were mounted on a base plate to aid positioning and alignment. The base plate leads to a drag increase and a drop in lift similar to adding surface roughness to a clean airfoil. The authors present corrected wind tunnel data but details about the model and tunnel dimensions are unavailable to verify those corrections.

3.4. AVATAR data set

The AVATAR data set consists of fully turbulent RANS simulations of very thick DU series airfoils, namely DU00W2350, DU00W2401, and DU600 (an artificially designed 60% thick airfoil), used in the root and inboard sections of the AVATAR 10 MW reference turbine [2]. The airfoils are equipped with VGs at 30% chord-wise location and inflow Reynolds numbers range from 7 million to 14 million. The CFD data is generated with the open source solver SU2 [24] and validated against other CFD and experimental tools in the AVATAR project [25].

4. Benchmark results

4.1. Establishing baseline performance

Since RFOIL is tuned for better polar calculations compared to XFOIL, a baseline first needs to be established to show the difference between airfoil polars from RFOIL and XFOIL. The VG model implementation in both solvers will thus be compared to the respective baseline of each solver. The parameters used for comparison against experimental data are the angle of attack for positive stall and the lift coefficient at stall. This is because the effect of the VG is usually quantified with how much it delays stall onset. Table 1 shows that RFOIL is more accurate than XFOIL in predicting the stall onset and the maximum lift before stall. The standard deviation for both solvers is similar, which indicates that the improvements in RFOIL compared to XFOIL are applicable to a wider range of airfoils and flow conditions. This is because the improvements in RFOIL are based on physical flow phenomena observed in rotating, high-lift, and thicker airfoils. This is important because Section 4.3 will describe how numerically tuned models like the current VG model have much higher variance and are more prone to numerical instability for a wide range of configurations compared to models that have a physical basis.

4.2. Implementing the model in RFOIL

The VG model was first tested against calculations for clean airfoils to verify whether the VG model performed as expected. VGs delay stall onset and provide a higher maximum lift by

Table 1: Comparing the performance of XFOIL and RFOIL for airfoils without VGs

Mean Error				**Standard Deviation of Error**			
CL max (relative)		**Stall Angle (absolute)**		**CL max (relative)**		**Stall Angle (absolute)**	
XFOIL	**RFOIL**	**XFOIL**	**RFOIL**	**XFOIL**	**RFOIL**	**XFOIL**	**RFOIL**
8.45%	4.75%	4.61	0.56	9.00%	10.5%	4.30	1.60

delaying flow separation. Thus, for each airfoil, the clean airfoil lift polars were compared to the lift polars with VGs. Additionally, the pressure distributions were compared at an angle of attack where the clean airfoil clearly stalls to verify the delay in stall onset. Figure 2 shows the effect of a VG of height $h_{VG}/c = 0.01$, length $l_{VG}/c = 0.038$, and inclination angle 15.5° placed at 30% chord on the stall onset and lift performance of an FFA-W3-301 airfoil at a Reynolds number of 3 million. Figure 2a shows that the clean FFA-W3-301 airfoil has experienced flow separation (indicated by the flat part of the C_P curve) at an angle of attack of 17° while the same with a VG has not experienced separation.

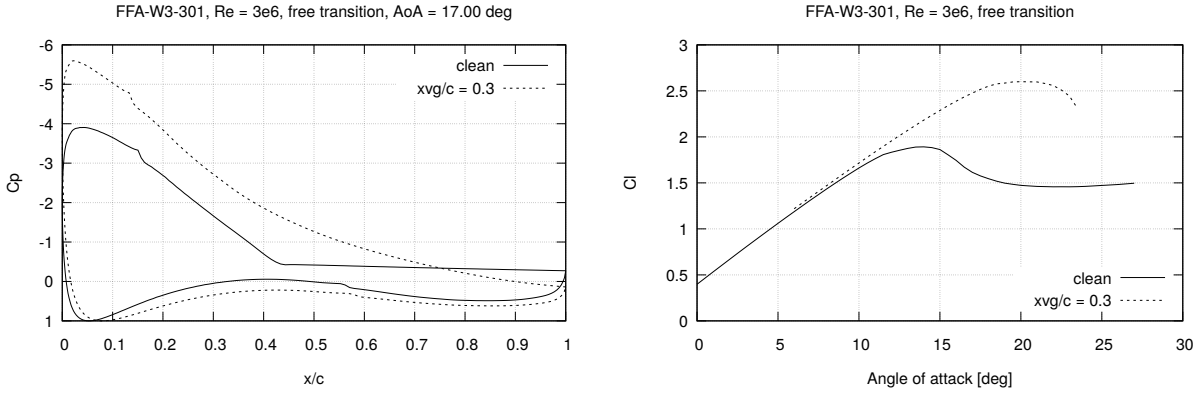

(a) VG prevents suction side flow separation at 17° (b) Stall onset is delayed by 6 degrees

Figure 2: A VG placed at $x/c = 0.3$ on an FFA-W3-301 airfoil delays flow separation and stall.

4.3. Benchmarking the VG model

Since the VG model is calibrated using a least squares multivariate regression approach, the baseline variance is established in Table 2 for both RFOILVG and XFOILVG by generating the polar statistics compared against the training data set of polars of several DU series airfoils. Follwing this, the difference between the calculated values from RFOILVG or XFOILVG and the reference wind tunnel and CFD datasets are presented in statistical form in Tables 3 to 6. The results are categorised in two ways — medium-thick and thick airfoils, and low and high Reynolds numbers. For thick airfoils and/or high Reynolds numbers, the results (wherever converged) were calculated by employing refinement of panels around the region of $0.05c$ upstream to $0.15c$ downstream of the VG location. This enabled obtaining polars for some numerically unstable cases, but not all. For most of these cases, the VG is too large, thus producing a source term S_{VG} so large that the solver cannot handle the gradient of the shear stress (see Equation (4)). The comparison between XFOILVG and RFOILVG shows that the trend of RFOIL being more accurate than XFOIL carries over into the VG model as well.

Table 2: Comparing the performance of RFOILVG and XFOILVG on the training data set of DU series airfoils to establish a base level of variance due to the least squares regression approach

Mean Error				**Standard Deviation of Error**			
CL max (relative)		**Stall Angle (absolute)**		**CL max (relative)**		**Stall Angle (absolute)**	
XFOILVG	**RFOILVG**	**XFOILVG**	**RFOILVG**	**XFOILVG**	**RFOILVG**	**XFOILVG**	**RFOILVG**
6.12%	1.03%	3.71	0.55	7.92%	3.74%	5.42	0.90

Table 3: Mean error in maximum lift and angle of attack of positive stall for RFOILVG and XFOILVG categorised by airfoil thickness

Airfoil Thickness	**Mean Error**			
	CL max (Relative)		**Stall Angle (Absolute)**	
	XFOIL	**RFOIL**	**XFOIL**	**RFOIL**
Medium thick (20% to 35%)	35.31%	23.26%	4.94	1.84
Thick (>36%)	6.47%	7.02%	1.75	1.53

Table 4: Standard deviation of error in maximum lift and angle of attack of positive stall for RFOILVG and XFOILVG categorised by airfoil thickness

Airfoil Thickness	**Standard Deviation of Error**			
	CL max (Relative)		**Stall Angle (Absolute)**	
	XFOIL	**RFOIL**	**XFOIL**	**RFOIL**
Medium thick (20% to 35%)	33.75%	30.53%	4.06	2.72
Thick (>36%)	17.74%	11.38%	5.44	2.14

Table 5: Mean error in maximum lift and angle of attack of positive stall for RFOILVG and XFOILVG categorised by Reynolds number

Reynolds Number	**Mean Error**			
	CL max (Relative)		**Stall Angle (Absolute)**	
	XFOIL	**RFOIL**	**XFOIL**	**RFOIL**
1 to 3 million	28.89%	18.04%	4.37	1.60
>3 million	-4.12%	17.66%	-0.88	3.17

Table 6: Standard deviation of error in maximum lift and angle of attack of positive stall for RFOILVG and XFOILVG categorised by Reynolds number

Reynolds Number	**Standard Deviation of Error**			
	CL max (Relative)		**Stall Angle (Absolute)**	
	XFOIL	**RFOIL**	**XFOIL**	**RFOIL**
1 to 3 million	31.82%	29.38%	4.06	2.62
>3 million	-4.12%	17.66%	-0.88	3.17

4.4. Computation time

The typical run times for a few selected airfoils and Reynolds numbers are compared with and without VG in Table 7. For each case, the computation time is the time taken to compute and save data for a polar from $-20°$ to $20°$ in steps of 0.5 and the number of angles converged from these 81 angles is also presented. The analysis is performed on a machine with an Intel Core i7 2.7 GHz processor, 32 GB RAM, and 1 TB SSD. It is expected that comparable machines will provide comparable run times. For thicker airfoils, the computation time is lower because the calculation converges for more of the very positive and very negative angles with the VG model since VGs keep the flow attached for longer compared to clean airfoils.

Table 7: Computation times of different types of airfoils at different Reynolds numbers with and without VGs

Case		**Computation Time**			
		Without VG		**With VG**	
Airfoil thickness	**Reynolds Number**	**Time (s)**	**Angles Converged**	**Time (s)**	**Angles Converged**
Medium thick (24%)	1.6 million	105.39	41/81	70.24	41/81
Thick (36%)	3 million	111.57	41/81	35.87	81/81
Thick (40%)	11 million	155.49	36/81	37.09	80/81

5. Reflection on the benchmark

Being a numerically calibrated model, it is evident that the VG model performs better for the airfoils it was calibrated on (Table 2) compared to a more general database of airfoils and VG configurations (Tables 3 and 5). In fact, the model can be viewed as *over-calibrated* because the mean error and variance for the VG model on the training data set (Table 2) even surpasses the mean error and variance of base RFOIL and XFOIL (Table 1). When it comes to variance of the results, the levels of variance of the VG model (Tables 4 and 6) when compared to base RFOIL and XFOIL (Table 1) are typical of models whose basis is numeric calibration compared to a physical basis.

The current VG model, while having a physical basis, is still a numerically calibrated model. Its high variance level means that it needs to be calibrated to a wider range of airfoils, flow conditions, and VG configurations. Such data is difficult to collect because both wind tunnel tests and CFD simulations for VGs are quite resource intensive. Meanwhile, the accuracy of the VG model also leaves much to be desired for. This is because modifying the IBL equations for added turbulence is not sufficient. While is true that VGs produce more turbulence in the boundary layer, Section 6 describes how this is just a by-product of the mixing process that involves redistribution of flow, and thus, is not the characteristic mechanism in itself. When comparing RFOILVG and XFOILVG, it is seen that RFOILVG is more accurate than XFOILVG in most cases, along with a smaller spread of the error value when it deviates from the reference data sets. This difference is largely attributed to the fact that the base version of RFOIL is already an improvement over the base version of XFOIL even before the VG model is implemented.

6. Future Work: A VG model characterising the mixing mechanism

As mentioned in Section 5, added turbulence in the boundary layer is actually a by-product of the mixing induced by VGs and not the characteristic mechanism behind the VGs. The mixing induced by VGs instead is a physical redistribution of flow by the vortices from the more energetic to the less energetic parts of the boundary layer. This results in a net mass

and momentum flux alongside an increased turbulence. This can be demonstrated clearly when the vortices downstream of VGs placed in boundary layers are analysed. To do this, RANS simulations of turbulent flat plates equipped with VGs were performed by the authors and validated against PIV measurements of the same presented in [26]. A preliminary study of the integral boundary layer characteristics shows that VGs modify the displacement thickness δ^* (Figure 3a), momentum thickness θ (Figure 3b), skin friction C_f (Figure 3c), kinetic energy shape factor H_k (Figure 3d), and the viscous dissipation coefficient $C_{\mathcal{D}}$ (Figure 4a), alongside the shear stress coefficient C_τ (Figure 4b). This means that modifying just the shear lag equation in the IBL framework is insufficient. To capture the mixing mechanism induced by the VGs, the momentum, kinetic energy, and turbulence equations (Equations (1) to (3)) need to be modified simultaneously. This approach is being studied by the authors of this paper and will be presented in future work.

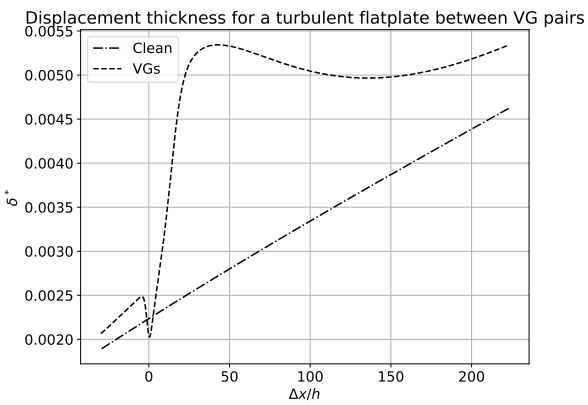

(a) Displacement thickness

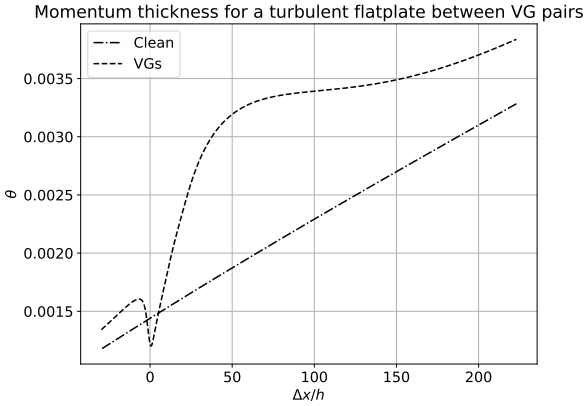

(b) Momentum thickness

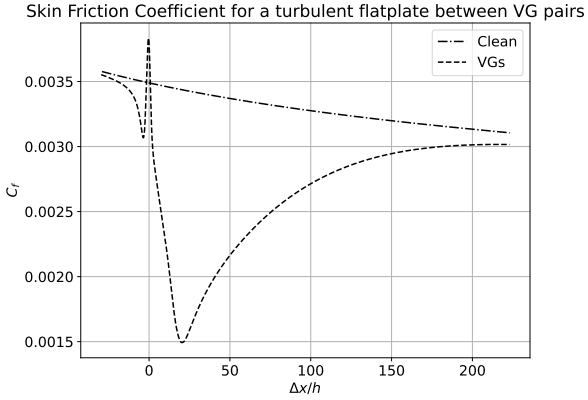

(c) Skin friction coefficient

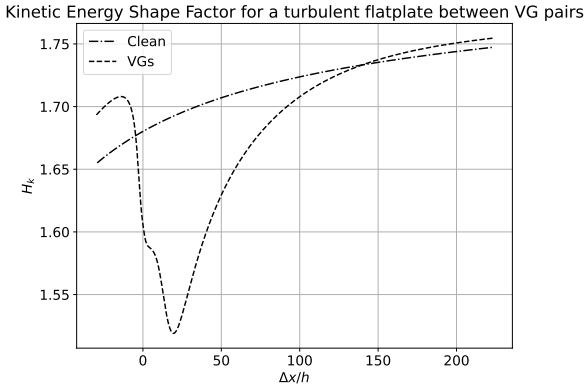

(d) Kinetic energy shape factor

Figure 3: VGs modify the momentum, kinetic energy, and turbulence properties of boundary layers

7. Conclusions

An extensive benchmark of the VG model developed for integral boundary layer methods shows the limitations of modelling the effect of VGs as just added turbulence in IBL methods. The numerically calibrated multi-variate regression approach would need a much larger training database of airfoil polars for all representative Reynolds numbers, airfoil thicknesses, and VG

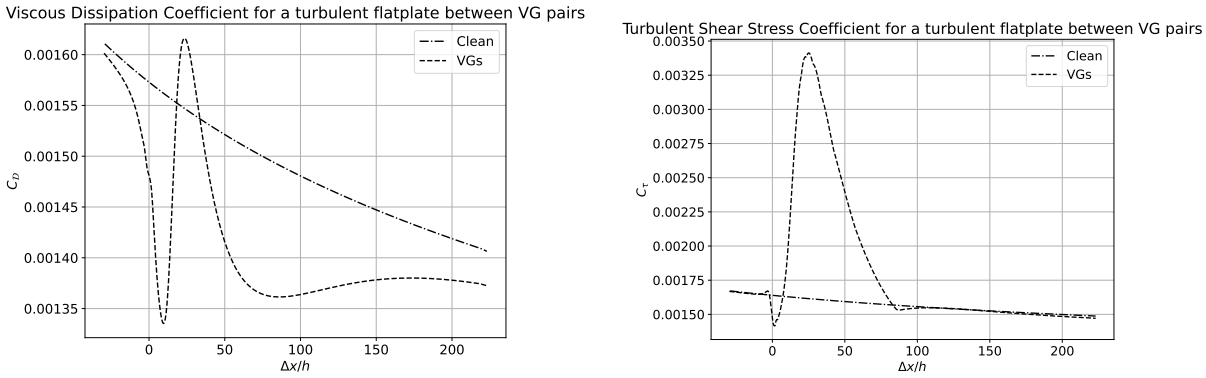

(a) Viscous dissipation coefficient (b) Turbulent shear stress coefficient

Figure 4: VGs modify the momentum, kinetic energy, and turbulence properties of boundary layers (contd.)

configurations. Such an extensive database is hard to come by because wind tunnel test campaigns and numerical simulations of airfoils with VGs are time and resource intensive. Instead, the authors of this paper propose an alternate line of investigation that captures the mixing induced modifications to the momentum, energy, and turbulence properties of boundary layers caused by vortex generators. Results of such an investigation will be presented in subsequent publications by the authors of this paper.

8. Acknowledgement of funding

This work was carried out in the VoGUe project funded by a Privaat-Publieke Samenwerkingentoeslag (PPS toeslag) granted by the Netherlands Enterprise Agency (RVO). Partners involved in the VoGUe project are TNO, TU Delft, and Vestas Wind Systems A/S.

References

[1] Jensen P H, Chaviaropolos T and Natarajan A 2017 *Innwind.eu* **325**

[2] Schepers J G, Ceyhan O, Savenije F J, Stettner M, Kooijman H J, Chaviarapoulos P, Sieros G, Simao Ferreira C S, Sørensen N, Wächter M, Stoevesandt B, Lutz T, Gonzalez A, Barakos G, Voutsinas A, Croce A and Madsen J 2015 *33rd Wind Energy Symposium* (American Institute of Aeronautics and Astronautics Inc.(AIAA)) pp 291–310 ISBN 9781624103445

[3] Grasso F and Ceyhan O 2015 *33rd Wind Energy Symposium* (Reston, Virginia: American Institute of Aeronautics and Astronautics) ISBN 978-1-62410-344-5

[4] McKenna R, Ostman P and Fichtner W 2016 *Renewable and Sustainable Energy Reviews* **53** 1212–1221 ISSN 18790690

[5] Schubauer G B and Spangenberg W G 1960 *Journal of Fluid Mechanics* **8** 10 ISSN 0022-1120

[6] Lin J C 2002 *Progress in Aerospace Sciences* **38** 389–420 ISSN 0376-0421

[7] Bender E E, Anderson B H and Yagle P J 1999 *3rd ASME/JSME Joint Fluids Engineering Conference* p 1 ISBN 0791819612

[8] Jirásek A 2005 *Journal of Aircraft* **42** 1486–1491 ISSN 15333868

[9] Drela M 1989 *Low Reynolds Number Aerodynamics* 54 ed Mueller T J (Berlin, Heidelberg: Springer Berlin Heidelberg) pp 1–12 ISBN 978-3-642-84010-4

[10] Rooij V R 1996 Modification of the boundary layer calculation in RFOIL for improved airfoil stall prediction

[11] Ramanujam G and Özdemir H 2017 *35th Wind Energy Symposium, 2017* (American Institute of Aeronautics and Astronautics Inc, AIAA) ISBN 9781624104565

[12] Ramanujam G, Özdemir H and Hoeijmakers H W M 2016 *Journal of aircraft* **53** 1844–1852 ISSN 0021-8669

[13] Snel H, Houwink R and Bosschers J 1993 *Netherlands Energy Research Foundation ECN* **93** 395–399

[14] Drela M 1986 Two-dimensional Transonic Aerodynamic Design and Analysis using the Euler Equations Tech. rep. URL `https://dspace.mit.edu/handle/1721.1/104732`

[15] Kerho M F and Kramer B R 2003 *41st Aerospace Sciences Meeting and Exhibit* p 211 ISBN 9781624100994

[16] De Tavernier D, Baldacchino D and Ferreira C 2018 *Wind Energy* **21** 906–921 ISSN 1095-4244

[17] Green J, Weeks D and Brooman J 1977 Prediction of Turbulent Boundary Layers and Wakes in Compressible Flow by a Lag-Entrainment Method Tech. Rep. 3791

[18] Swafford T W 1983 *AIAA journal* **21** 923–926 ISSN 0001-1452

[19] Baldacchino D, Ferreira C, Tavernier D D, Timmer W A and Van Bussel G J W 2018 *Wind Energy* **21** 745–765 ISSN 1095-4244

[20] Timmer W A and van Rooij R P J O M 2003 *Journal of Solar Energy Engineering* **125** 488–496 ISSN 0199-6231

[21] Van Ingen J L 2008 *38th AIAA Fluid Dynamics Conference and Exhibit*

[22] Fuglsang P L, Antoniou I, Dahl K and Madsen H A 1998 *Riso-Reports-Riso R* **1041** 1–163 ISSN 0106-2840

[23] Sørensen N N, Zahle F, Bak C and Vronsky T 2014 *Journal of Physics: Conference Series* **524** 012019 ISSN 1742-6596

[24] Economon T D, Palacios F, Copeland S R, Lukaczyk T W and Alonso J J 2016 *AIAA Journal* **54** 828–846 ISSN 00011452

[25] Manolesos M and Prospathopoulos J 2015 *Avatar Task 3.1 Report* 1–106

[26] Baldacchino D, Ragni D, Simao Ferreira C and van Bussel G 2015 *45th AIAA Fluid Dynamics Conference* p 3345